Journal of Sound and Vibration 577 (2024) 118336

Contents lists available at ScienceDirect

Journal of Sound and Vibration

journal homepage: www.elsevier.com/locate/jsvi

Free vibration of variable-thickness plates via adaptive finite elements

Martino C. Moruzzi [a,*,1], Maria Cinefra [b,**,1], Sara Bagassi [a,1]

[a] Department of Industrial Engineering, Università di Bologna, Italy
[b] Department of Mechanics, Mathematics and Management, Politecnico di Bari, Italy

ARTICLE INFO

Keywords:
Adaptive finite elements
Natural frequency
Variable-thickness plate
Free vibrations

ABSTRACT

New technologies, such as additive manufacturing combined with topology optimisation or bio-inspired design, can produce lightweight structures with better dynamical properties but more complex geometries. Analysing these components with the finite element method can become time-consuming because of fine 3D meshes. By exploiting the node-dependent kinematic approach of Carrera's unified formulation and using Lagrange expanding functions, this work presents the implementation of adaptive finite elements for the free-vibration analysis of plates with an arbitrary thickness variation through the in-plane domain. In other words, the kinematics of the 2D model on which the element is based can be adapted to the geometry of the plate. The formulation is mainly based on the 3D integration of the approximating functions and computation of a 3D Jacobian matrix inside the element for the derivation of stiffness and mass matrices; substantially, the resulting elements are 3D elements in which the order of expansion through the thickness can be different from that in the plane of the plate. The free vibration analysis of some plates with different thickness variations is performed. The results demonstrate that the present elements allow us to accurately study these innovative 2D structures by employing much fewer degrees of freedom with respect to classical 3D finite elements.

1. Introduction

New technologies in structural optimisation lead to new geometries and shapes. Additive manufacturing combined with topology optimisation or bio-inspired design can obtain and produce very disruptive structures with better dynamical properties and lower weight. Nevertheless, there is still a lack of numerically accurate, flexible, and computationally cheap methods to study these newly generated structures. This gap increases if we consider unconventional structures as plates with variable thickness.

In this work, we focus on free vibrations of plates, where the possibility to optimise the structure's thickness leads to variation in the structure's stiffness and mass [1]. The dynamic analysis of plates with a given thickness variation across the mid-surface can be convenient for attenuating vibrations in thin-walled structures. Several structures can belong to this class of shells and plates, such as some aerodynamic surfaces or structural panels of aircraft (e.g., a fuselage panel in [2]) and spacecraft (e.g., a load-carrying structure in [3]), and others from several fields (e.g., a gas tank in [4] and a plate for ballistic impact application in [5]). However, the thickness variation in a plate can play a key role in the acoustic behaviour of structures coupled to fluid cavities. The method

* Correspondence to: Department of Industrial Engineering Università di Bologna, Via Fontanelle, 40, 47121 Forlì, Italy.
** Correspondence to: Department of Mechanics, Mathematics and Management Politecnico di Bari, Via Orabona, 4, 70125 Bari, Italy.
E-mail addresses: martinocarlo.moruzz2@unibo.it (M.C. Moruzzi), maria.cinefra@poliba.it (M. Cinefra).
[1] All authors participated equally in the development of the work presented in the article and in its writing.

https://doi.org/10.1016/j.jsv.2024.118336
Received 13 October 2023; Received in revised form 22 January 2024; Accepted 6 February 2024
Available online 7 February 2024

presented and validated in this article may become very useful in investigating new solutions for noise reduction (e.g., sandwich or generally multi-layer plates with varying thickness) in several fields, such as noise reduction in aircraft or acoustic loads in spacecraft.

To extract the natural frequencies of a plate with a variable thickness, several numerical and analytic methods are proposed, not only in the FEM framework, for different types of thickness variation. Some of them will be discussed in the validation process, and they are summarised below:

- stepped variation of the thickness for a rectangular plate solved with an extended Kantorovich method by Cortinez et al. [6] or by Singhatanadgid et al. [7];
- the linear variation of the thickness for a rectangular plate is studied by Sanzi et al. [8], and for an orthotropic plate by Civalek [9] and Malhotra et al. [10], and for a symmetrically laminated plate with an extended Kantorovich method by Fallah et al. [11]. Analytical solutions can be found in the work by Tash et al. [12];
- for a circular plate, there are several works on linear (or double linear) and exponential radial thickness variation, such as those by Singh et al. [13,14] or Wu et al. [15] and Azimi [16,17]. Other works on circular plates with a variation in thickness are those by Wang et al. [18], by Bahmyari et al. [19], and by Vasiliev et al. [20].

In this framework, the Finite Element Method (FEM) remains the most convenient tool to study the dynamic behaviour of structures with complex geometries due to its flexibility in the analysable range of geometry. Considering the current numerical finite element methods, plates with variable thicknesses can be studied only using 3D elements, entailing a large computational effort due to the limits on the aspect ratio of the elements themselves. The method presented here aims to extend the advantages of the so-called Carrera's Unified Formulation (CUF) [21] to variable-thickness plates, thus using 2D elements and significantly reducing the computational cost. This reduction becomes even more important in fluid–structure interfaces, as in the classical vibro-acoustic problem for studying noise reduction in the acoustic cavity.

The CUF was introduced to overcome the limitations of the classical 2D models in describing the through-the-thickness kinematics of composite plate structures by employing a hierarchical, unified, and compact notation [21]. In particular, a new approach, called Node-Dependent Kinematics (NDK), has been recently developed in this framework to improve the numerical efficiency of the CUF models while maintaining their accuracy very high [22,23]. Thanks to this formulation, FEM models with variable 'nodal' kinematics can be built conveniently. However, all these CUF models, as well as classical plate models [24–27], are formulated on some basic assumptions of the initial undeformed body: constant thickness through all the in-plane domain of the 2D finite element. The FEM study of plates with arbitrary thickness variation requires a new two-dimensional modelling approach.

This work aims to propose a reliable method to study plates with variable thickness independent of the type of thickness variation (analytical or numerical function, random, etc.). To obtain these results, we develop adaptive finite elements in the framework of CUF, which enables a wide class of plate elements thanks to the split of the three-dimensional displacement field into a two-dimensional one on the plate plane and a one-dimensional field along the thickness.

The adaptive finite elements are based on the following idea: the integrals computed inside the stiffness and mass matrices of the dynamic governing equations involve new 3D approximating functions of the element that are the combination of two-dimensional shape functions of the FEM and through-the-thickness functions of the CUF. The main benefit of these elements is the possibility of refining the model where the geometrical features of the component – for example, where the thickness increases – or the kinematic behaviour of the plate requires that. Finally, these elements can be seen as 3D elements in which the order of expansion in one direction (the thickness) can be different from that in the other two directions (the midsurface), allowing a reduction of the computational cost with respect to classical 3D elements. Two preliminary works by the authors show the possible advantages of adaptive finite elements for variable-thickness plates and shells [28] and for multi-layer cylindrical shells for noise reduction [29]. Therefore, the purpose of this work is to extend the adaptive finite elements, which have already been introduced in [30,31], to the analysis of variable-thickness plates and to carry out an exhaustive validation of these elements by showing their advantages in comparison with classical 3D elements.

The article is arranged as follows: in Section 2, the 2D models based on CUF and Lagrange expansion are briefly recalled, and then the formulation of adaptive finite elements in the framework of the NDK approach is presented; the derivation of governing equations from Hamilton's principle is explained in Section 3; Section 4 contains the assessment of the models by comparison with some study cases from the literature that demonstrate the capabilities of the present elements; Section 5 reports the free-vibration analysis of some plates with complex variations of the thickness by highlighting the effect on natural frequencies; finally, Section 6 summarises the conclusions of this work.

2. Adaptive finite elements

This section presents the formulation of adaptive finite elements, starting from the presentation of the classical 2D CUF approximation along the thickness and the 2D FEM modelling in the framework of CUF. The combination of CUF and FEM in new 3D approximating functions gives rise to the present elements. In particular, Section 2.2 highlights the differences with respect to the regular 2D finite elements formulated based on CUF.

As will be demonstrated by the results, these finite elements significantly reduce degrees of freedom in the modelling of variable-thickness plates with respect to classical 3D finite elements. These last employ the same order of expansion in all the spatial directions, and this limits the choice of the aspect ratio of the elements by leading to an excessive refinement of the mesh. On the contrary, the present elements keep the same degrees of freedom as 2D elements but work as 3D elements and preserve the same accuracy.

2.1. 2D kinematic models based on CUF

In two-dimensional models, Carrera's unified formulation (see [21]) approximates the kinematic field along the thickness of the plate in a unified manner that is then used to derive the governing equations in a very compact way and makes the method very easy to implement. This formulation represents a huge improvement with respect to classical theories, which hold several limitations in the simulation of complex structures. Many of these limitations lay on the kinematic description that should be theoretically enriched with an infinite number of terms (see Washizu [32]) to avoid physical inconsistencies and take high-order effects into account. This approach is often not applicable to the study of real problems because of the computational cost. There is a need to truncate the approximating expansion of the primary mechanical variables along the thickness to a given order. Furthermore, the more terms in the kinematics, the higher the analysis cost. Carrera's unified formulation solves these issues, deriving the governing equations in a compact and unified manner and allowing a systematic formulation of a series of 2D models.

According to CUF 2D modelling, the displacement field of a generic plate structure, whose mid-surface lies on the plane $x-y$ and the thickness goes along z, can be described as a generic expansion of the generalised displacements by employing arbitrary functions of the thickness coordinate:

$$\mathbf{s}(x,y,z) = F_\tau(z)\mathbf{s}_\tau(x,y) \quad \tau = 1,2,\dots,M \tag{1}$$

where $\boldsymbol{s} = \{u, v, w\}$ is the 3D displacements field and $\boldsymbol{s}_\tau = \{u_\tau, v_\tau, w_\tau\}$ is the vector of generalised displacements, function of the midsurface coordinates, M is the number of terms in the expansion, τ is a summation index, and the arbitrary functions $F_\tau(z)$ characterise the 2D model. Indeed, depending on the choice of the thickness functions $F_\tau(z)$, different classes of 2D theories can be implemented among these classical theories, such as Kirchhoff–Love, Reissner–Mindlin, and so on. In this work, only Lagrange polynomials are considered thickness functions, for reasons that will be clear later, but other types of functions, such as Taylor or Legendre polynomials, can also be conveniently adopted, as shown in many previous works by Carrera et al. [21,22].

Two-dimensional theories based on Lagrange expansion are formulated by employing 1D Lagrange polynomials as F_τ thickness functions:

$$\begin{aligned} u &= F_1(\zeta)\, u_1 + F_\tau(\zeta)\, u_\tau \\ v &= F_1(\zeta)\, v_1 + F_\tau(\zeta)\, v_\tau \\ w &= F_1(\zeta)\, w_1 + F_\tau(\zeta)\, w_\tau \end{aligned} \tag{2}$$

where τ goes from 2 to $p+1$, where p is the desired order of the thickness function F_τ, and ζ is an adimensional coordinate along the thickness direction that ranges from -1 to 1. According to this, two-node (linear) LW1, three-node (parabolic) LW2, and four-node (cubic) LW3 expansions can be used.

Displacement fields like Lagrange-based ones have been employed in previous authors' works to implement layer-wise models. Lagrange polynomials have also been used in the formulation of shell theories with variable kinematics by Kulikov and his co-workers. The readers can refer to the papers [33,34] for more details about 2D models based on Lagrange expansions.

2.1.1. 2D finite element approximation

In the case of plate models, the approximation of the generalised displacements on the mid-surface of the plate is performed employing the finite element method, according to 2D shape functions $L_i(\xi,\eta)$ and the unknown nodal displacements $\mathbf{S}_{\tau i}$:

$$\mathbf{s}_\tau(x,y) = L_i(\xi,\eta)\mathbf{S}_{\tau i}, \qquad i = 1,2,\dots,n_{ele} \tag{3}$$

where n_{ele} is the number of nodes per element, and the vector of unknown nodal displacements is

$$\mathbf{S}_{\tau i} = \left\{ \begin{array}{ccc} U_{\tau i} & V_{\tau i} & W_{\tau i} \end{array} \right\}^{\mathrm{T}} \tag{4}$$

Lagrange interpolating polynomials have been used in this work to define the finite element. Their expression is not provided here, but one can find it in the book by Carrera et al. [21], where four-node (Q4), nine-node (Q9), and sixteen-node (Q16) 2D elements are described.

The FEM approximation can be combined with the kinematic assumptions of Carrera's unified formulation in the following expression of the 3D displacement field:

$$\mathbf{s} = F_\tau L_i \mathbf{S}_{\tau i} \tag{5}$$

the functions F_τ and L_i depend on the 2D kinematic model and the element type, respectively.

In the above expression (Eq. (5)), the shape functions L_i and the thickness functions F_τ are independent. Recently, Carrera et al. [22] introduced a coupling between them by making the expanding function F_τ dependent on the shape function L_i, as follows:

$$\mathbf{s} = F_\tau^i L_i \mathbf{S}_{\tau i} \tag{6}$$

The difference between Eqs. (6) and (5) is the additional superscript i of the thickness function F_τ, which is also the index of the shape function L_i. This fact introduces a dependency on the kinematic assumption from the FE node, namely the Node-Dependent Kinematic (NDK) approach.

It is well known that increasing the polynomial order of expanding functions allows an accurate approximation of the structure response. By exploiting the NDK, the kinematic model can be chosen on specific nodes with the possibility of performing a local adaptable refinement of the approximation without any compatibility requirement for the nodal kinematic.

2.2. CUF and FEM combined in a new 3D approximation

In the framework of the NDK approach, it is possible to extend the 2D models of the CUF to the description of plates with variable thickness by combining the CUF kinematic assumption and the FEM approximation in a unique 3D function, as follows:

$$\mathbf{s} = (F_\tau^i L_i)\mathbf{S}_{\tau i} = N_{\tau i}(\xi,\eta,\zeta)\mathbf{S}_{\tau i} \tag{7}$$

where ξ,η,ζ are the natural coordinates corresponding to x,y,z. In this equation, $N_{\tau i} = (F_\tau^i L_i)$ represents a 3D approximating function with different polynomial expansion orders in different spatial directions. Similarly, the virtual variation of 3D displacements, which will be used later to derive the governing equations, can be expressed as:

$$\delta\mathbf{s} = (F_s^j L_j)\delta\mathbf{S}_{sj} = N_{sj}(\xi,\eta,\zeta)\delta\mathbf{S}_{sj} \tag{8}$$

where new summation indexes s and j have been introduced.

According to this formalism, the volume integrals of the 3D approximating functions involved in the governing equations are not split into 1D and 2D integrals, as usual in 2D elements. Still, they are computed directly in the 3D domain. The 3D Gauss rule is used to perform the integrals involved in the governing equations, and the Jacobian matrix from natural coordinates ξ,η,ζ to global coordinates x,y,z is computed in 3D form.

Concerning the work [30], the Gauss rule for the numerical solution of volume integrals is here adapted to the maximum polynomial order of approximating functions in the different spatial directions; that is, the number of Gauss points along a certain coordinate (ξ, η, or ζ) is chosen according to the maximum polynomial order in that coordinate. This allows us to consider any arbitrary thickness variation without loss of accuracy. More details about governing equations and related integrals are provided below.

3. Governing equations

As stated above, the CUF permits the writing of the governing equations and the related finite element arrays in a compact way that is characterised by the definition of fundamental nuclei, which are formally invariant with respect to the F_τ and L_i functions. The mathematical derivation of the fundamental nuclei of the stiffness and mass matrix in the case of the present adaptive elements is provided in detail.

The same reference system and notation as in Section 2.1 are used. According to Voigt notation, often adopted in classical elasticity, stress and strain tensors can be arranged in six-term vectors that read, respectively:

$$\begin{aligned}\boldsymbol{\sigma}^{\mathrm{T}} &= \left\{ \begin{array}{cccccc} \sigma_{yy} & \sigma_{xx} & \sigma_{zz} & \sigma_{xz} & \sigma_{yz} & \sigma_{xy} \end{array} \right\} \\ \boldsymbol{\varepsilon}^{\mathrm{T}} &= \left\{ \begin{array}{cccccc} \varepsilon_{yy} & \varepsilon_{xx} & \varepsilon_{zz} & \gamma_{xz} & \gamma_{yz} & \gamma_{xy} \end{array} \right\}\end{aligned} \tag{9}$$

Considering these expressions, the geometrical relations between strains and displacements can be defined using a compact vectorial notation:

$$\boldsymbol{\varepsilon} = \mathbf{b}\,\mathbf{u} \tag{10}$$

where, in the case of geometrically linear problems (small deformations and angles of rotations), $\mathbf{b}$ contains the following differential operator:

$$\mathbf{b} = \begin{bmatrix} 0 & \frac{\partial}{\partial y} & 0 \\ \frac{\partial}{\partial x} & 0 & 0 \\ 0 & 0 & \frac{\partial}{\partial z} \\ \frac{\partial}{\partial z} & 0 & \frac{\partial}{\partial x} \\ 0 & \frac{\partial}{\partial z} & \frac{\partial}{\partial y} \\ \frac{\partial}{\partial y} & \frac{\partial}{\partial x} & 0 \end{bmatrix} \tag{11}$$

On the other side, the relationship between stresses and strains for isotropic materials is written through the well-known Hooke's law:

$$\boldsymbol{\sigma} = \mathbf{C}\,\boldsymbol{\varepsilon} \tag{12}$$

where $\mathbf{C}$ is the matrix of the elasticity coefficients of the material

$$\mathbf{C} = \begin{bmatrix} C_{11} & C_{12} & C_{12} & 0 & 0 & 0 \\ C_{12} & C_{11} & C_{12} & 0 & 0 & 0 \\ C_{12} & C_{12} & C_{11} & 0 & 0 & 0 \\ 0 & 0 & 0 & C_{44} & 0 & 0 \\ 0 & 0 & 0 & 0 & C_{44} & 0 \\ 0 & 0 & 0 & 0 & 0 & C_{44} \end{bmatrix} \tag{13}$$

The coefficients of this matrix depend only on the Young's modulus, E, and the Poisson ratio, ν, and they are computed as:

$$\begin{aligned} C_{11} &= \frac{(1-\nu)E}{(1+\nu)(1-2\nu)} \\ C_{12} &= \frac{\nu E}{(1+\nu)(1-2\nu)} \\ C_{44} &= \frac{E}{2(1+\nu)} \end{aligned} \tag{14}$$

The governing equations for the free-vibration analysis are derived from Hamilton's principle (or the dynamic version of the principle of virtual displacements) that imposes, if the external forces are neglected, that the sum of the virtual variation of the internal work and the virtual variation of the inertial work has to be equal to zero:

$$\delta L_{\text{int}} + \delta L_{\text{ine}} = 0 \tag{15}$$

The internal work is equivalent to the elastic strain energy

$$\delta L_{\text{int}} = \int_V \delta \boldsymbol{\epsilon}^{\text{T}} \boldsymbol{\sigma} \, dV \tag{16}$$

where V is the volume of the domain. By substituting the constitutive equations (Eq. (12)), the geometrical relations (Eq. (10)) and the approximation of displacements given in Eqs. (7) and (8), the internal work can be rewritten as:

$$\delta L_{\text{int}} = \delta \mathbf{S}_{\tau i}^{\text{T}} \mathbf{K}^{\tau s i j} \mathbf{S}_{s j} \tag{17}$$

where $\mathbf{K}^{\tau s i j}$ is the 3×3 fundamental nucleus of the stiffness matrix.

According to Hamilton's principle, the inertial work can be expressed as:

$$\delta L_{\text{ine}} = \int_V \delta \mathbf{s}^{\text{T}} \rho \ddot{\mathbf{s}} \, dV \tag{18}$$

By adopting the FEM discretisation in Eq. (8) and the CUF kinematic assumption in Eq. (7), the intertial work becomes:

$$\delta L_{\text{ine}} = \delta \mathbf{S}_{\tau i}^{\text{T}} \mathbf{M}^{\tau s i j} \ddot{\mathbf{S}}_{s j} \tag{19}$$

where $\mathbf{M}^{\tau s i j}$ is the 3×3 fundamental nucleus of the mass matrix.

The fundamental nucleus formulations of the stiffness matrix $\mathbf{K}^{\tau s i j}$ and the mass matrix $\mathbf{M}^{\tau s i j}$ are reported in Appendix.

One should note that the expressions of the matrix components in the fundamental nuclei are invariant with respect to the choice of the thickness functions F_τ and the shape functions L_i, which both determine the numerical accuracy of the model. This means that any plate element can be automatically developed by simply expanding the fundamental nuclei according to the indexes τ, s, i, and j.

3.1. Acronyms

In this work, linear, quadratic, and cubic Lagrange-type shape functions are used for both F_τ and L_i functions. By summarising, the acronyms LW1 (linear, two nodes), LW2 (quadratic, three nodes), and LW3 (cubic, four nodes) indicate the 1D discretisation through the thickness of the plate; the nodes must be equally spaced; on the other hand, the acronyms Q4 (linear), Q9 (quadratic), and Q16 (cubic) are used for the 2D approximation on the mid-surface of the plate. A visual summary of the different LWn approaches is reported in Fig. 1. Thanks to the adaptive finite element formulations, it is possible to use a mixed approach, such as LW2-3, which combines quadratic (LW2) and cubic (LW3) Lagrange-type thickness functions in the same mesh. The merging of the nodes on the plate's plane and the plate's thickness generates the 3D adaptive finite element.

In CUF coding, the expansion order is set as a free input of the model by determining the number of degrees of freedom to be solved, and, thanks to the adaptive finite elements, the kinematic field along the thickness can be enriched only in the zone of interest, for example, where the plate is thicker.

4. Numerical validation

Free vibration analysis is performed for different rectangular and circular plates to validate the adaptive finite element formulation for variable-thickness plates and compared to literature results. The function, which describes the thickness, is usually half the plate thickness. The natural frequency extraction is done with MUL2 software,[2] developed by *Politecnico di Torino*. The software exploits the CUF extended with adaptive finite elements.

4.1. Rectangular plate

The validation process starts by studying a rectangular plate with a variable thickness. The constant thickness plate has already been studied in the CUF framework [35–38]. The free vibrations are compared to two literature models. The plate is modelled with 20×20 Quad9 quadratic square elements as sketched in Fig. 3(a).

[2] The software, based on the CUF, is available on the website: http://www.mul2.polito.it/. The version integrated with the adaptive finite elements is available by contacting the authors.

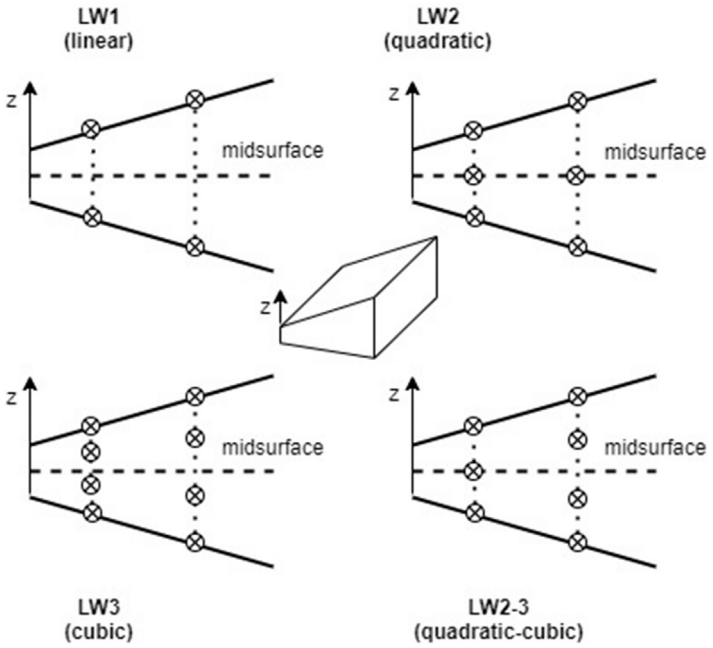

Fig. 1. The different LWn approaches are reported for a plate with a linear thickness variation: LW1, LW2, LW3, and the mixed LW2-3.

The first model is a plate with a stepped variation of thickness, studied by Cortinez et al. [6] with a Kantorovich extended method and by Sanzi et al. [8] with the finite element method. The plate geometry is reported in Fig. 2, and the thickness assumes two different values, h_1 and h_2, on the x-coordinate for a total length a. Parameter c defines the length of the first thickness value h_1.

The second plate has a linear variation in thickness, and it was studied by Bhat et al. [39] with a model based on the Rayleigh–Ritz method with characteristic orthogonal polynomial shape functions. The plate geometry and structure are reported in Fig. 2, and the following equation describes the thickness:

$$h(x) = h_0 \left[(\alpha/a)x + 1\right] \tag{20}$$

in which a is the plate length over which the thickness is increased with respect to the x-coordinate, α is the rate of increase, and h_0 is the minimum thickness of the plate. A similar plate has already been studied and compared to a 3D element model in the work by Cinefra [30].

The two plates are studied for two boundary conditions applied to the four edges, simply supported and clamped. The two analyses extract the non-dimensional natural frequency coefficients of the two systems:

$$\Omega^2 = \frac{\rho h}{D_0}\omega^2 a^4 \tag{21}$$

where ρ is the material density, and $D = Eh^3/\left[12(1-\nu^2)\right]$ is the bending stiffness, which depends on Young's modulus E and the Poisson's ratio $\nu = 0.3$. The reference thickness h corresponds to h_1 for the first case and to h_0 for the second case.

4.2. Circular plate

The circular plate in Fig. 4 with variable thickness is studied by comparing the natural frequency coefficients in Eq. (21) with two literature cases, including three different thickness variations. The circular plate is modelled with 1874 Quad9 elements, as sketched in Fig. 3(b).

The first case is based on the work by Wu et al. [15], where the authors study the free vibrations of a plate with two variable thickness functions exploiting a generalised differential quadrature rule and compare the results with those obtained with the Rayleigh–Ritz-based method and by Azimi [16,17] with a receptance method. The two thicknesses are a function of the plate radial coordinate r:

- a linear function

$$h(r) = h_0(1 + \eta r) \tag{22}$$

- an exponential function

$$h(r) = h_0 e^{\eta r} \tag{23}$$

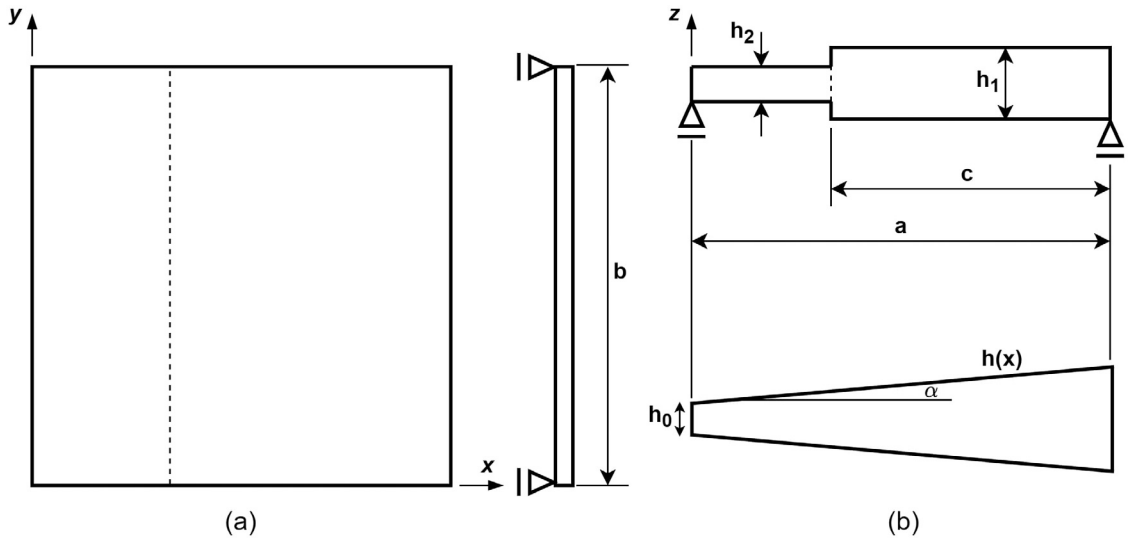

Fig. 2. The rectangular plate geometries used in the validation for the simply supported case. (a) Top view (where the dotted line indicates the thickness change in the stepped plate). (b) Thickness section for the two plates: the stepped thickness plate in [6] and the plate with a linear increase in thickness in [39].

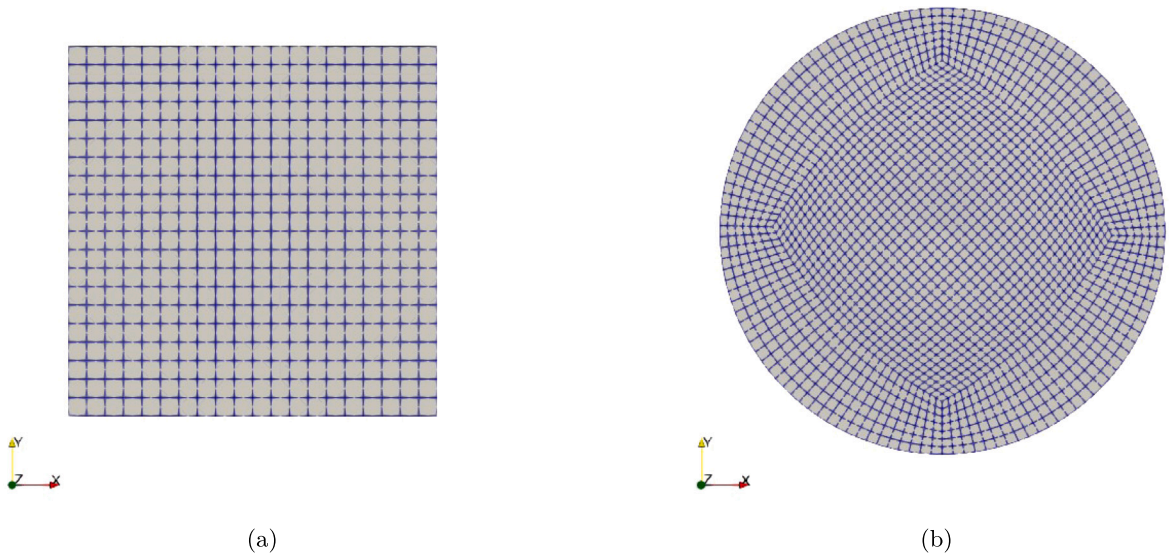

Fig. 3. The Quad9 element distribution on the plate plane. (a) Square plate. (b) Circular plate.

The plates are tested for different boundary conditions (free, simply supported, and clamped) and the rate of increase (or decrease) parameter, η. Therefore, h_0 is the reference thickness, and, depending on the sign of η, it can be the maximum or minimum thickness. According to [15], we studied the two cases with $\eta = \pm 0.3$ for the linear function and $\eta = \pm 1$ for the exponential function.

The second case studies a plate with a parabolic variation of the thickness based on the work by Harris [40], where the frequencies are calculated by the mean of an exact solution. The thickness varies according to the following parabolic law:

$$h = h_0 \left(1 - \iota^2\right) \tag{24}$$

and $\iota = r/r_0$, which is the adimensional radial coordinate of r normalised on the plate radius r_0. In this case, h_0 is the maximum thickness, while on the edges there is a sharp corner. The plate has a free-edge boundary condition.

The natural frequency coefficients are defined for the rectangular plate case.

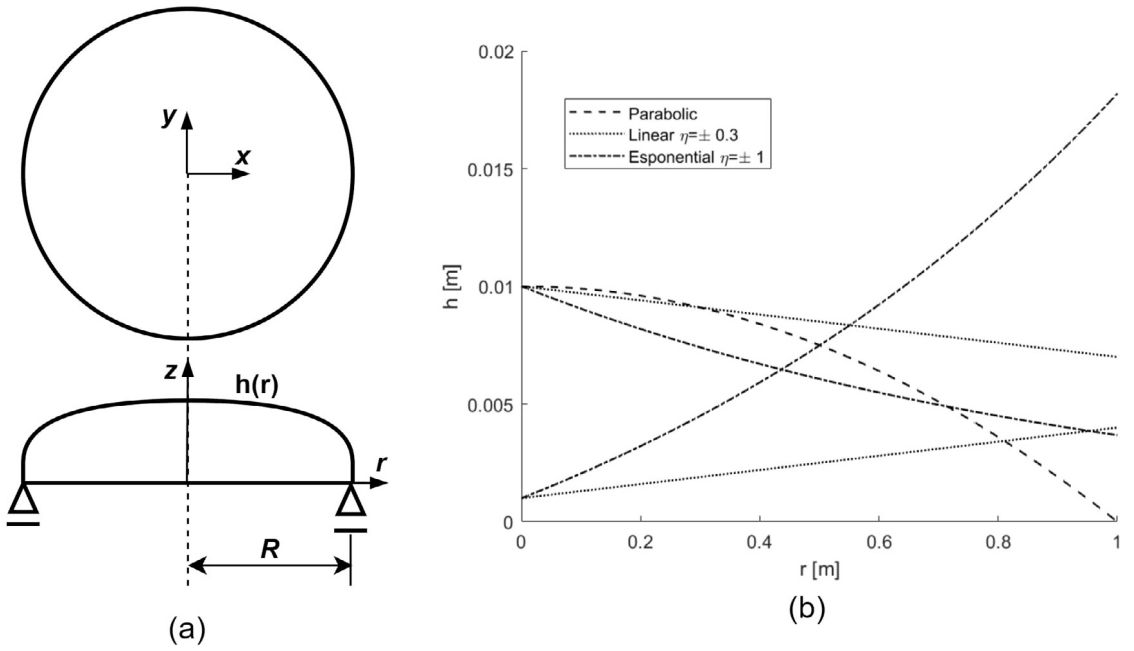

Fig. 4. The circular plate geometries used in the validation. (a) Top and half of the side view. (b) The different thickness sections defined on half of the circle studied in [15,40].

4.3. Comparison with 3D elements

We extract the natural frequencies for two plates with a variable thickness based on sinusoidal functions to show the advantages of adaptive finite elements. The two examples presented in this section, the square plate with a double sine variation and the circular plate with a sine wave, have never been studied in the literature, as far as the authors know. Therefore, the only possible comparison of the results is with commercial software that exploits 3D elements. The purpose of these two examples is to demonstrate the computational advantage of adaptive finite elements. The choice of the sinusoidal variations in thickness is due more to the shape assumed by the plates themselves than to the possibility of a real application. Indeed, they present a periodic and significant variation in thickness, an extreme case to demonstrate the potential of the method presented in the article and the limitations of 3D elements.

For the rectangular plate in Fig. 5, the thickness is defined by a double sine function:

$$h(x, y) = \alpha \sin(\beta x) \sin(\beta y) + h_0 \tag{25}$$

where h_0 is the reference thickness, α a scale parameter, and β defines the number of periods of the sine function. A simply supported boundary condition is applied to the four edges. In this case, the choice of different β leads to different thicknesses at edges where the boundary conditions are used, as shown by comparing Fig. 5(c) and Fig. 5(d) for $x = \pm 0.5$ m.

For the circular plate in Fig. 6, the thickness is defined by a circular wave function:

$$h(r) = \alpha \sin\left(\beta \pi r^2\right) + h_0 \tag{26}$$

where the term β is multiplied by π to have a full or half period in the radius length. A simply supported boundary condition is applied at the edge. In this case, the number π guarantees always having the same thickness at the edges. The number of half periods is a whole number, as shown in Fig. 6(c), where the sine develops for half a period along the radius, and in Fig. 6(d), where it develops for three periods.

The plates are made of the same material, aluminium (Young's modulus $E = 70$ GPa, Poisson's ratio $\nu = 0.35$, and density $\rho = 2700$ kg/m^3). The reference thickness is equal to $h_0 = 0.0105$ m and the scale parameter to $\alpha = 0.01$ to have an important thickness variation, from $h_{min} = 0.0005$ m to $h_{max} = 0.0205$ m (we are as before referring to the half thickness). The parameter β is considered a variable in order to study the different dynamic behaviour of the plates for a different number of sinusoidal periods.

According to previous validations, the two structures are studied through the LW2 and LW3 approaches, and thanks to the adaptive finite element formulation with a mixed approach, LW2-3, if it is necessary.

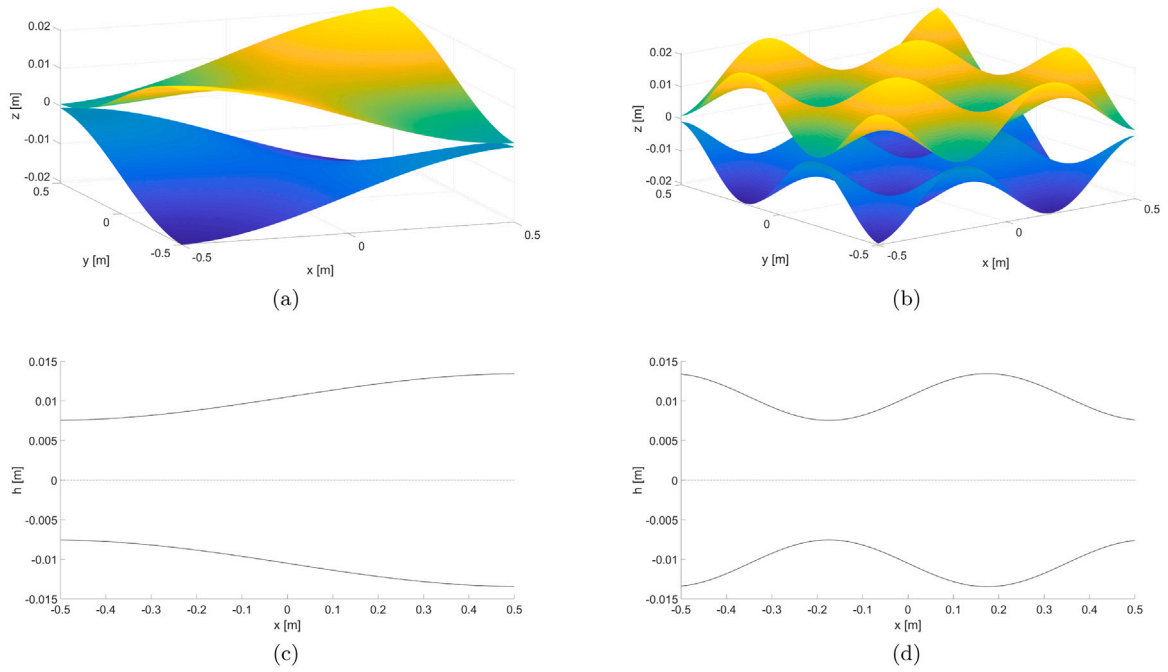

Fig. 5. The rectangular plate with a double sinusoidal thickness for two different periods according to the parameter β. (a) Top and bottom surface $\beta = 3$. (b) Top and bottom surface $\beta = 9$. (c) Section at $y = 0.1$ m for $\beta = 3$. (d) Section at $y = 0.1$ m for $\beta = 9$.

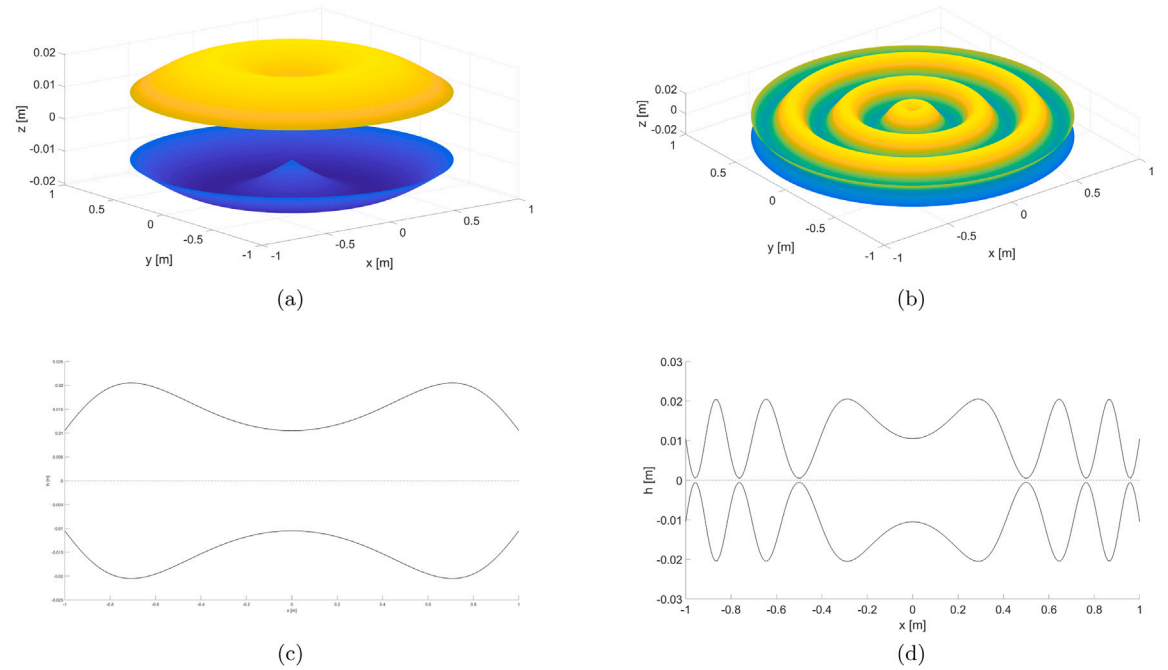

Fig. 6. The circular plate with a radial sinusoidal thickness for two different periods according to the parameter β. (a) Top and bottom surface $\beta = 1$. (b) Top and bottom surface $\beta = 6$. (c) Section for $\beta = 1$. (d) Section for $\beta = 6$.

Table 1
Fundamental frequency coefficient Ω of a simply supported square plate with discontinuously varying thickness.

h_2/h_1	$c/a = 0.5$					$c/a = 0.8$				
	LW2	LW2–3	LW3	[6]	[8]	LW2	LW2–3	LW3	[6]	[8]
0.8	17.58	17.58	17.57	17.77	17.67	18.91	18.83	18.83	18.99	18.95
0.6	15.31	15.30	15.30	16.11	15.38	17.90	17.66	17.66	18.23	17.79

Table 2
Fundamental frequency coefficient Ω of a clamped square plate with discontinuously varying thickness.

h_2/h_1	$c/a = 0.5$					$c/a = 0.8$				
	LW2	LW2–3	LW3	[6]	[8]	LW2	LW2–3	LW3	[6]	[8]
0.8	32.31	32.31	32.30	32.3	32.4	34.65	34.60	34.59	34.5	34.7
0.6	28.17	28.17	28.16	28.9	28.3	33.04	32.87	32.87	33.3	32.02

Table 3
Frequency coefficients Ω_i of a plate with linear thickness and simply supported boundary conditions.

Ω_i	$\alpha = 0$				$\alpha = 0.2$				$\alpha = 0.4$			
	LW2	LW3	Analyt.	[39]	LW2	LW2-3	LW3	[39]	LW2	LW2-3	LW3	[39]
Ω_1	19.7049	19.6975	19.7392	19.7392	21.6444	21.6398	21.6348	21.6920	23.5445	23.5366	23.5323	23.6092
Ω_2	49.3479	49.3271	49.3480	49.3481	54.1751	54.1661	54.1071	54.1607	58.8635	58.6951	58.6783	56.7687
Ω_3	49.3479	49.3271	49.3480	49.3481	54.1325	54.1257	54.1494	54.2047	58.7087	58.8494	58.8321	58.9283
Ω_4	78.8342	78.7905	78.9568	78.9569	86.5560	86.5367	86.5009	86.7528	94.0947	94.0613	94.0267	94.3773
Ω_5	99.0110	98.9483	98.6960	99.3042	108.3528	108.6175	108.5591	108.7610	116.9178	116.8959	117.8427	117.4410
Ω_6	99.0114	98.9490	98.6960	99.3042	108.6339	108.3447	108.2788	108.9320	117.9305	117.8892	116.8331	118.1150

Table 4
Frequency coefficients Ω of a plate with linear thickness and clamped boundary conditions.

Ω_i	$\alpha = 0$			$\alpha = 0.2$				$\alpha = 0.4$			
	LW2	LW3	[39]	LW2	LW2–3	LW3	[39]	LW2	LW2-3	LW3	[39]
Ω_1	36.2161	36.2059	35.9855	39.7488	39.7468	39.7365	39.5097	43.1569	43.1518	43.1422	42.9088
Ω_2	74.0204	73.9824	73.3947	81.1459	81.2007	81.1006	80.5194	87.9083	88.1374	87.8555	87.2835
Ω_3	74.0204	73.9824	73.3947	81.2143	81.1431	81.1691	80.5857	88.1584	87.8950	88.1051	87.5259
Ω_4	109.0440	108.9835	108.2180	119.6663	119.6503	119.5926	118.8650	129.9869	129.9469	129.8984	129.2150
Ω_5	133.2354	133.1199	131.7790	145.8779	145.8650	145.7419	144.4620	157.4929	157.4627	157.3377	156.1420
Ω_6	133.8653	133.7501	132.4100	146.6304	146.6017	146.4944	145.1900	158.9078	158.8398	158.7494	157.4210

5. Results

5.1. Rectangular plate

For the multi-step square plate in [6,8], different geometries are studied, changing the thicknesses of the two steps and the length, so the parameters h_2/h_1 and c/a. The fundamental frequencies for the two boundary conditions, simply supported and clamped, are reported in Tables 1 and 2, respectively. The results are very similar to those from the literature, both for LW2 (DoF 15129), LW3 (DoF 20172), and the mixed approach LW2-3 (DoF 17589 for $c/a = 0.5$ and 19065 for $c/a = 0.8$). The mixed approach uses LW2 expansion in the thinnest step and LW3 in the thickest.

For the second case in [39], the first six frequency coefficients Ω are calculated for the two boundary conditions (Table 3 for simply supported edges and Table 4 for clamped edges), using LW2, LW3, and a mixed approach LW2-3. The criterion depends on the parameter α in Eq. (20), which corresponds to the percentage of plate length modelled with an LW3 approach, corresponding to the thickest portion. Three cases are studied: $\alpha = 0$, so a constant thickness plate, in this case for SS boundary conditions, the results are compared to the well-known analytical solution; $\alpha = 0.2$, so in the mixed approach, the 20% of the plate length is modelled with an LW3 expansion (DoF 16236); $\alpha = 0.4$ with 40% of LW3 in the mixed approach (DoF 17220). The results are very similar to those from the literature for all three approaches.

5.2. Circular plate

For the circular plate, the baseline structure with constant thickness is validated because, to the authors' knowledge, there is not any work that studies this kind of plate in the CUF framework. The validation is performed by comparing the results based on the analytical solution based on Bessel functions with those obtained by Wu et al. [15] and Azimi [16]. The results are reported in Table 5 for three boundary conditions applied on the edges (free, simply supported, and clamped). The LW2 (68607 DoF) and LW3 (91476 DoF) approaches are validated. Once the baseline geometry is validated to avoid any preliminary error, the validation for

Table 5
The first six natural frequency coefficients $\Omega_{m,k}$ (the symmetrical modes are merged) comparison for the constant thickness plate with different boundary conditions. In the table, m is the number of radial nodal lines and k is the number of circumferential nodal lines, according to [15].

	m,k	Analytical	[15]	[16]	LW2	LW3
Free	0, 2	5.382	5.358	5.358	5.359	5.359
	1, 0	9.003	9.003	9.003	9.007	9.006
	0, 3	12.461	12.439		12.439	12.437
	1, 1	20.475	20.475	20.475	20.484	20.482
	0, 4		21.835		21.836	21.832
	0, 5	34.716	33.495	4.935	33.499	33.491
Simply supported	0, 0	4.935	4.935	4.935	5.018	5.017
	0, 1	13.898	13.898	13.898	13.976	13.974
	0, 2	25.613	25.613	25.613	25.680	25.694
	1, 0	29.720	29.720	29.720	29.816	29.811
	0, 3	39.957	39.957		40.033	40.023
	1, 1	48.481	48.479	48.479	48.602	48.591
Clamped	0, 0	10.211	10.216	10.216	10.237	10.232
	0, 1	21.261	21.260	21.260	21.313	21.299
	0, 2	34.881	34.877	34.877	34.948	34.927
	1, 0	39.771	39.771	39.771	39.903	39.875
	0, 3	51.022	51.030		51.172	51.131
	1, 1	60.824	60.829	60.829	61.047	60.998

Table 6
The first six natural frequency coefficients $\Omega_{m,k}$ comparison (the symmetrical modes are merged) for a plate with a linear variation of the thickness for different boundary conditions. In the table, m is the number of radial nodal lines and k is the number of circumferential nodal lines, according to [15].

	$\eta = -0.3$				$\eta = 0.3$				
	m,k	[15]	[17]	LW2	LW3	m,k	[15]	[17]	LW2	LW3
Free	0, 2	4.380		4.647	4.647	0, 2	5.973		6.167	6.166
	1, 0	7.951	7.951	7.955	7.954	1, 0	10.132	10.134	10.136	10.136
	0, 3	9.786		10.034	10.033	0, 3	14.791		14.946	14.943
	0, 4	16.978		17.036	17.034	1, 1	23.533		23.584	23.581
	1, 1	17.281		17.355	17.354	0, 4	26.592		26.726	26.721
	0, 5	25.380		25.641	25.637	2, 0	44.064		44.090	44.083
Simply supported	0, 0	4.116	4.116	4.202	4.202	0, 0	5.748	5.748	5.828	5.827
	0, 1	11.194		11.368	11.367	0, 1	16.368		16.490	16.487
	0, 2	20.539		20.743	20.741	0, 2	30.413		30.535	30.544
	1,0	24.727	24.728	24.845	24.842	1,0	34.562	34.562	34.641	34.635
	0, 3	31.639		31.891	31.886	0, 3	47.934		48.052	48.037
	1, 1	40.162		40.361	40.354	1, 1	56.364		56.488	56.469
Clamped	0, 0	7.779	7.778	7.807	7.806	0, 0	12.663	12.663	12.693	12.690
	0, 1	16.638		16.783	16.781	0, 1	25.607		25.726	25.716
	0, 2	27.611		27.823	27.819	0, 2	41.762		41.920	41.906
	1,0	32.462	32.463	32.638	32.631	1,0	46.780	46.784	46.925	46.906
	0, 3	40.256		40.597	40.588	0, 3	61.313		61.554	61.529
	1, 1	49.852		50.194	50.180	1, 1	71.196		71.449	71.426

Table 7
The first six natural frequencies coefficient $\Omega_{m,k}$ comparison (the symmetrical modes are merged) for a plate with an exponential variation of the thickness for different boundary conditions. In the table, m is the number of radial nodal lines and k is the number of circumferential nodal lines, according to [15].

	$\eta = -1$					$\eta = 1$				
	m,k	[15]	[17]	LW2	LW3	m,k	[15]	[17]	LW2	LW3
Simply supported	0, 0	2.846	2.845	2.952	2.952	0, 0	9.005	9.007	9.082	9.076
	1, 0	17.224	17.224	17.403	17.401	1, 0	51.290	51.331	51.310	51.296
	2, 0	43.354	43.357	43.739	43.727	2, 0	123.985	124.630	123.835	123.772
	3, 0	81.271	81.288	80.803	80.775	3, 0	228.178	236.800	227.584	227.377
Clamped	0, 0	4.765	4.764	4.791	4.784	0, 0	23.235	23.239	23.259	23.220
	1, 0	22.052	22.051	22.229	22.204	1, 0	72.457	72.505	72.487	72.324
	2, 0	51.127	51.129	51.748	51.690	2, 0	152.914	153.450	152.765	152.355
	3, 0	91.986	91.995	91.100	90.991	3, 0	264.980	271.180	264.214	263.380

two different variable-thickness plates is performed and compared to literature results [15,17]. The differences between the LW2 and LW3 approaches are small; therefore, the mixed approach is not used. In Table 6, the results are reported for a linear variation, and in Table 7, for an exponential one.

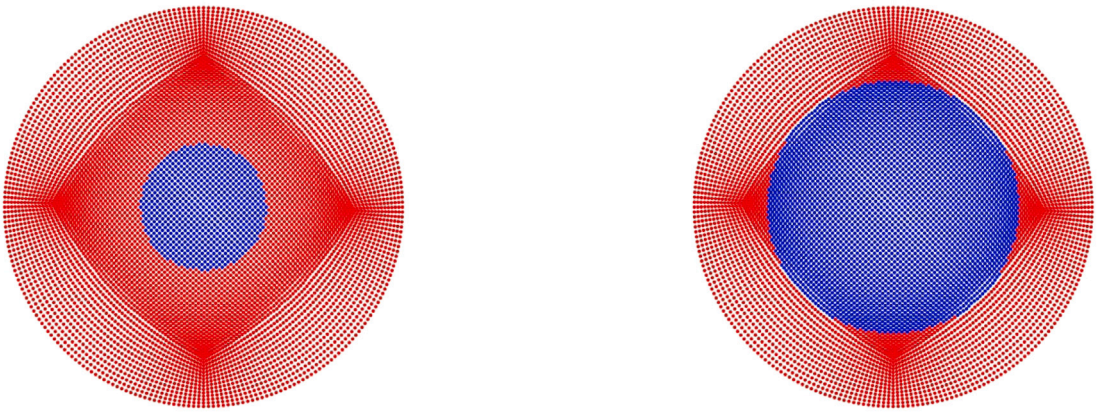

Fig. 7. The nodal maps of the different LW approaches exploited in a mixed LW2-3 model for the circular plate with a parabolic thickness (red for the LW2 and blue for the LW3). The maps report the percentage of the plate studied with an LW3 approach. (a) 20%. (b) 80%.

Table 8
The first ten natural frequency coefficients $\Omega_{m,k}$ comparison for a plate with a parabolic variation of the thickness and free edges. In the table, m is the number of radial nodal lines and k is the number of circumferential nodal lines, according to [40].

m, k	[40]	LW2	LW2-3 20%	LW2-3 80%	LW3
1, 2	5.80	5.80	5.79	5.79	5.79
1, 0	9.67	9.67	9.66	9.66	9.66
0, 3	10.04	10.04	10.03	10.03	10.03
0, 4	14.20	14.20	14.18	14.18	14.18
1, 1	17.80	17.79	17.76	17.76	17.76
0, 5	18.33	18.34	18.30	18.30	18.30
0, 6	22.45	22.47	22.42	22.42	22.42
1, 2	25.88	25.89	25.80	25.80	25.80
2, 0	29.83	29.82	29.72	29.71	29.71
1, 3	33.94	33.96	33.83	33.82	33.82

Finally, the adaptive finite elements are validated by comparing the results with those obtained by Harris [40]. The particularity of the plate in Harris' work is the presence of a corner on the edge of the circular plate. Therefore, at the edge, the expansion nodes collapse on the mean surface. In this case, we also use two different mixed approaches, LW2-3 (73456 DoF for the 20% of the radius of the plate and 87702 for the 80%), where the criterion is the percentage of the plate radius, that uses an LW3 expansion. The nodal maps show the different approaches distribution and are reported in Fig. 7. The results are documented in Table 8.

The results are, in general, in good agreement with the literature results for both the LW2 and LW3 approaches. This conclusion validates the formulation. Nevertheless, the increase in accuracy with respect to the square plate is also due to the smaller size of the elements. We use almost 68000 DoF with an LW2 approach to mesh a surface of π m^2 while for the plate, around 15000 DoF are used for 1 m^2 surface. The high number of DoF in the circle model is used to not deform the Q9 elements. In other studies, the formulation is expanded for deformed elements too [31].

5.3. Comparison with 3D elements

The first case studies a plate with a thickness based on a double sine function, Eq. (25). The analysis is split into three steps:

- upstream of the comparisons, a convergence analysis was performed for the 3D elements in order to understand for which DoF number the solid FEM model converged to a solution. The results for $\beta = 9$ are reported in Table 9, and the case with 46968 is chosen thanks to the convergence analysis;
- a comparison of the first six frequency coefficients between the LW approaches and a 3D element model for $\beta = 9$. The 3D element model is built and solved by the commercial software Ansys,[3] and made of 20-node hexahedral elements, Hexa20. The mixed approach LW2-3 uses a criterion based on the plate's maximum thickness. If the local thickness is higher than a percentage of the maximum one, it switches from three to four-node expansion, as shown in Fig. 8, where the plate is mapped

[3] https://www.ansys.com/

Table 9
Results in terms of Ω of the convergence analysis for the square plate with $\beta = 9$ and modelled with solid elements. The result used in the following comparisons is highlighted.

DoF	7689	19 893	31 023	46 968	72 051	231 552
1	19.39	17.94	17.80	17.48	17.48	17.48
2	51.47	46.74	46.16	45.18	45.17	45.17
3	57.74	51.55	50.98	49.99	49.99	49.98
4	91.98	79.83	78.81	76.81	76.79	76.78
5	104.64	88.36	86.41	83.26	83.25	83.23
6	105.18	88.69	86.73	83.52	83.50	83.48

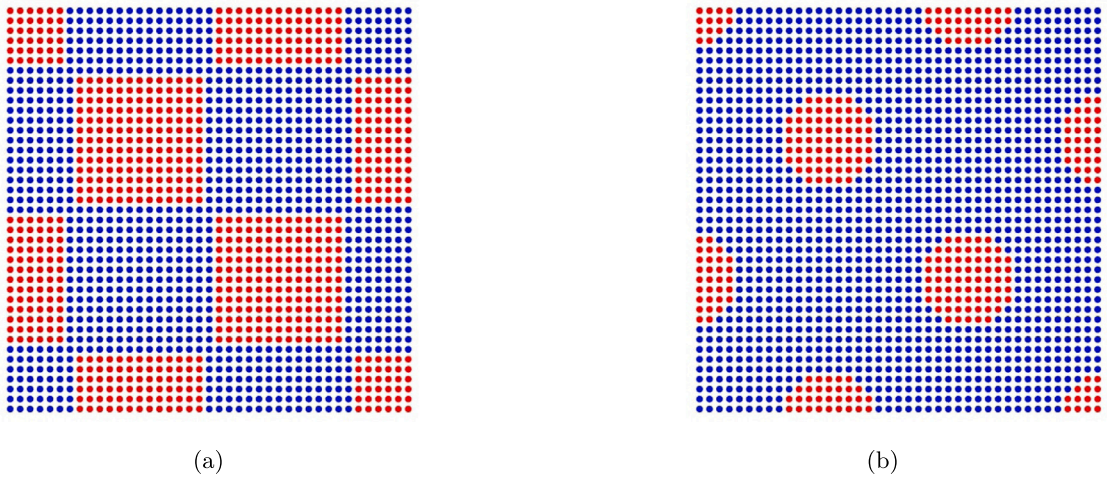

Fig. 8. The nodal maps of the different LW approaches exploited in a mixed LW2-3 model for the square plate with a double sinusoidal thickness (red for the LW2 and blue for the LW3). The maps report the two criteria for the thickness used in the analysis. (a) 50% with LW3. (b) 75% with LW3.

Table 10
The first six frequencies coefficients Ω of a simply supported plate with a double sine function ($\beta = 9$) for the thickness. The results are compared between LW approaches and 3D elements.

Modes	LW2	LW2-3 50%	LW2-3 75%	LW3	3D
1	17.48	17.48	17.48	17.56	17.53
2	45.18	45.17	45.17	45.37	45.32
3	49.99	49.99	49.98	50.47	50.35
4	76.81	76.79	76.78	77.56	77.36
5	83.26	83.25	83.23	84.33	84.42
6	83.52	83.50	83.48	84.57	84.16
DoF	15 129	18 006	19 320	20 172	46 968

according to the different LW approaches in the two studied cases (50% and 75% of the maximum thickness). The results are reported in Table 10. The 3D model, despite the increase in the number of elements (and DoF), converges to values similar to those of the shell model for almost three times the DoF of the LW2 model and more than two times for the LW3 model. The reason is the plate thickness variation, which starts from 0.001 m to 0.041 m, forcing the use of very small 3D elements. The differences between the different LW approaches are small. Nevertheless, with a mixed approach, which uses four nodes (LW3) for thickness higher than 50% of the maximum one, it is possible to have almost the same accuracy as an LW3 model, saving more than 10% of DoF;

- the influence of the parameter β on the plate's dynamic behaviour is studied by comparing the first three frequency coefficients for different values of β. The results are reported in Table 11 and compared to a plate with a constant thickness equal to the average. The specific volume of each model is reported as the ratio between the variable-thickness plate volume V and the constant-thickness plate volume V_0. The fundamental frequency coefficient changes according to the different stiffnesses and masses. For the case $\beta = 5$, it is possible to obtain a high value of Ω, with the lowest volume (and mass), while for $\beta = 3$, the mass is equal to the mass of a constant thickness plate, but there is an increase in Ω. The first mode for $\beta = 9$ is compared to the constant thickness plate in Fig. 9.

In the second case, the circular simply supported plate with a sinusoidal thickness is studied similarly to the square plate. The convergence analysis is reported in Table 12. However, due to the high complexity of the thickness variation and circular shape, the convergence is not completely obtained despite the high number of DoF. The results from a 3D model are compared to those

Table 11
The first three frequency coefficients Ω and volumes for different β of a square plate with a double sinusoidal thickness variation. A mixed LW2-3 approach is used (except for the constant thickness plate), switching from LW2 to LW3 when half of the thickness is reached.

Modes	β				Constant
	3	5	7	9	
1	14.21	14.25	12.90	12.10	19.60
2	27.17	31.09	36.13	31.28	49.03
3	37.60	36.66	52.58	34.74	78.10
V/V_0	0.9979	0.9650	0.9916	0.9980	1

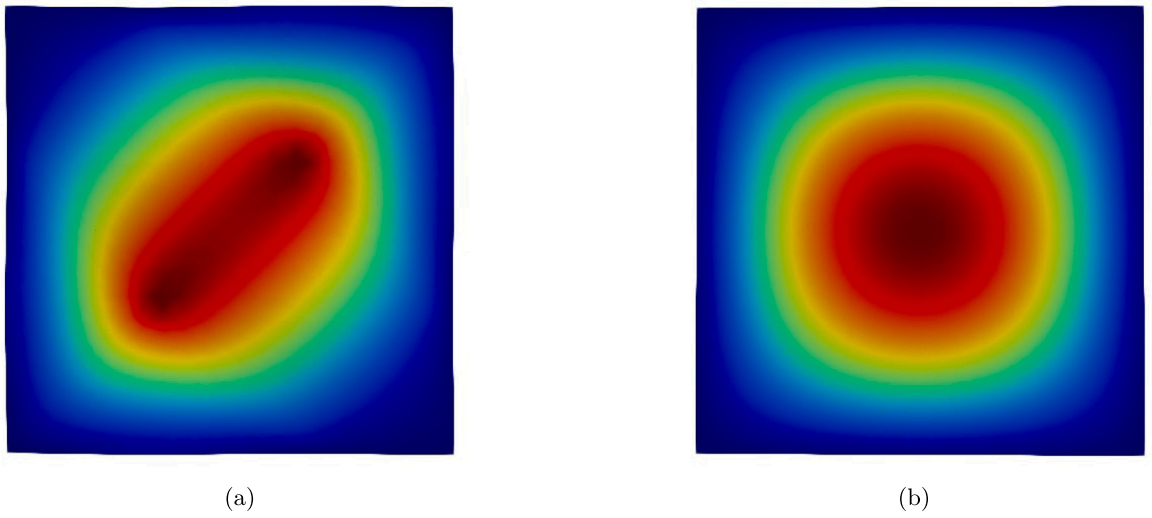

Fig. 9. The first mode for a simply supported square plate with $\nu = 0.35$. (a) Double sinusoidal thickness with $\beta = 9$. (b) Constant thickness equal to the average of the double sinusoidal one.

Table 12
Results in terms of Ω of the convergence analysis for the circular plate with $\beta = 2\pi$ and modelled with solid elements. The result used in the following comparisons is highlighted.

DoF	31 179	51 078	78 861	157 860	194 637
1	2.64	2.14	1.88	1.58	1.49
2	6.71	5.47	4.88	4.15	3.84
3	7.03	5.66	4.96	4.16	3.89
4	26.89	25.73	24.87	23.52	20.04
5	27.22	25.80	24.95	24.20	23.42
6	33.39	29.64	25.88	24.21	23.80

obtained with the proposed formulation for $\beta = 2\pi$. Moreover, the influence of the parameter β in Eq. (26) is studied. The parameter varies from π to 6π. According to the previous results, due to the small differences between the LW2 and LW3 approaches, the mixed expansion LW2-3 is not exploited for this problem. The comparison with 3D elements is reported in Table 13. The 3D model, despite the high number of DoF due to the deformation of the Hexa20 elements, is not completely able to understand the dynamic behaviour of the plate. The reason for the square plate is the thickness variation, which varies from 0.001 m to 0.041 m. In Table 14 is reported the comparison of the different natural frequency coefficients for different periods of thickness function Eq. (26). The fundamental frequency is strongly influenced by the shape of the thickness, which influences both the mass and stiffness of the structure. The first mode for $\beta = 6\pi$ is compared to the constant thickness plate in Fig. 10.

6. Conclusions

The adaptive finite elements can accurately describe the dynamic behaviour of variable-thickness plates without being influenced by the shape of the plate or the thickness pattern, wisely choosing the different numbers of expansion points along the thickness (e.g., the LWn approach) according to the local requirements and shape of the structure (local thickness, type of material, local loads, etc.). Moreover, they allow us to save thousands of degrees of freedom with respect to 3D elements, usually implemented by conventional FEM approaches. Finally, the adaptive finite elements are used to analyse the free vibration of two plates with a

Table 13
The first six frequency coefficients Ω of a simply supported plate with a sinusoidal function ($\beta = 2\pi$) for the thickness. The results are compared between LW approaches and 3D elements.

Modes	LW2	LW3	3D
1	1.51	1.50	1.49
2	3.56	3.56	3.84
3	3.58	3.57	3.89
4	16.92	16.87	20.04
5	20.13	20.06	23.42
6	20.37	20.31	23.80
DoF	68 607	91476	194 637

Table 14
The first three frequency coefficients Ω and volumes for different β and LW approaches of a circular plate with a radial sinusoidal thickness variation. The expansion uses three nodes on the thickness and a quadratic functions (LW2).

Modes	β						Constant
	π	2π	3π	4π	5π	6π	
1	8.35	1.51	4.46	2.33	5.16	3.48	5.02
2	23.85	3.56	10.22	4.57	12.00	6.90	13.97
3	41.45	16.92	12.69	11.26	17.48	14.04	25.70
V/V_0	1.1930	1	1.0643	1	1.0386	1	1

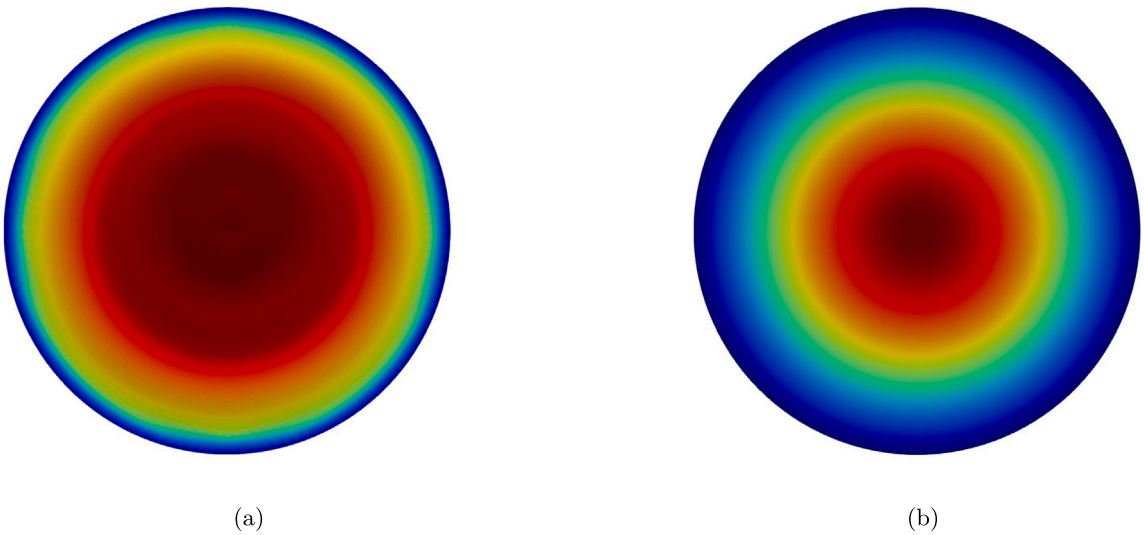

Fig. 10. The first mode for a simply supported circular plate with $\nu = 0.3$. (a) Radial sinusoidal thickness with $\beta = 6\pi$. (b) Constant thickness equal to the average of the sinusoidal one.

sinusoidal thickness to demonstrate the formulation's power. The effect of the period of the sinusoidal function on the dynamics of the plate is assessed. In fact, in the first part of the article, the method presented is validated by comparing the results with those available in the literature, while in the second part, a comparison is made with 3D elements. Sinusoidal functions for the plate's thickness are chosen to have a periodic variation of thickness, starting from a minimum of a few millimetres to a maximum in the order of centimetres. Beyond the results on the dynamic behaviour of these structures, this research aimed to show how adaptive finite elements can study any plate with varying thickness in a simple and computationally cheap way (compared to 3D elements, less than 50% of the DoF were used). Unlike 3D elements, adaptive finite elements, in addition to using less DoF, allow a simpler mesh generation process, being entirely similar to that used for 2D elements in the case of constant plates. In contrast to 3D elements, variable thickness plates may present convergence problems due to the significant variation in thickness.

The formulation presented in this article is limited to flat plates; however, an extension to shells with curvature using curvilinear elements, such as the cylinder studied in [29], is possible. Furthermore, the formulation can be extended for vibro-acoustic problems in the creation of fluid–structure interfaces [31,38], or with the application of the method of Rayleigh integrals [41] to study the transmission loss of plates with variable thickness [42]. Finally, the adaptive finite element formulation can work for beams with a variable section.

In conclusion, this work demonstrates, through case studies, how it is possible to use this new class of elements, the adaptive finite elements, to study the mechanical behaviour of any type of variable-thickness plate, from those obtainable by topological optimisation to some aerodynamic surfaces of an aircraft or rocket, up to the bulkheads of gas tanks, aircraft, or spacecraft.

CRediT authorship contribution statement

Martino C. Moruzzi: Conceptualization, Data curation, Formal analysis, Investigation, Methodology, Resources, Software, Validation, Visualization, Writing – original draft, Writing – review & editing. **Maria Cinefra:** Conceptualization, Data curation, Formal analysis, Investigation, Methodology, Resources, Software, Supervision, Validation, Visualization, Writing – original draft, Writing – review & editing. **Sara Bagassi:** Conceptualization, Data curation, Methodology, Supervision, Writing – original draft, Writing – review & editing.

Declaration of competing interest

We wish to confirm that there are no known conflicts of interest associated with this publication and there has been no significant financial support for this work that could have influenced its outcome.

Data availability

Data will be made available on request.

Appendix. Stiffness and mass matrices in the governing equations

The fundamental nuclei of the stiffness and mass matrices are reported according to the previous notation in Section 3.
The 3×3 fundamental nucleus of the stiffness matrix $\mathbf{K}^{\tau sij}$ is defined by its nine terms:

$$
\begin{aligned}
\mathbf{K}_{xx}^{\tau sij} &= C_{22}\int_V \left(L_i F_\tau\right)_{,x}\left(L_j F_s\right)_{,x} dV + C_{44}\int_V \left(L_i F_\tau\right)_{,z}\left(L_j F_s\right)_{,z} dV + C_{66}\int_V \left(L_i F_\tau\right)_{,y}\left(L_j F_s\right)_{,y} dV \\
\mathbf{K}_{xy}^{\tau sij} &= C_{23}\int_V \left(L_i F_\tau\right)_{,y}\left(L_j F_s\right)_{,x} dV + C_{66}\int_V \left(L_i F_\tau\right)_{,x}\left(L_j F_s\right)_{,y} dV \\
\mathbf{K}_{xz}^{\tau sij} &= C_{12}\int_V \left(L_i F_\tau\right)_{,z}\left(L_j F_s\right)_{,x} dV + C_{44}\int_V \left(L_i F_\tau\right)_{,x}\left(L_j F_s\right)_{,z} dV \\
\mathbf{K}_{yx}^{\tau sij} &= C_{23}\int_V \left(L_i F_\tau\right)_{,x}\left(L_j F_s\right)_{,y} dV + C_{66}\int_V \left(L_i F_\tau\right)_{,y}\left(L_j F_s\right)_{,x} dV \\
\mathbf{K}_{yy}^{\tau sij} &= C_{33}\int_V \left(L_i F_\tau\right)_{,y}\left(L_j F_s\right)_{,y} dV + C_{55}\int_V \left(L_i F_\tau\right)_{,z}\left(L_j F_s\right)_{,z} dV + C_{66}\int_V \left(L_i F_\tau\right)_{,x}\left(L_j F_s\right)_{,x} dV \\
\mathbf{K}_{yz}^{\tau sij} &= C_{13}\int_V \left(L_i F_\tau\right)_{,z}\left(L_j F_s\right)_{,y} dV + C_{55}\int_V \left(L_i F_\tau\right)_{,y}\left(L_j F_s\right)_{,z} dV \\
\mathbf{K}_{zx}^{\tau sij} &= C_{12}\int_V \left(L_i F_\tau\right)_{,x}\left(L_j F_s\right)_{,z} dV + C_{44}\int_V \left(L_i F_\tau\right)_{,z}\left(L_j F_s\right)_{,x} dV \\
\mathbf{K}_{zy}^{\tau sij} &= C_{13}\int_V \left(L_i F_\tau\right)_{,y}\left(L_j F_s\right)_{,z} dV + C_{55}\int_V \left(L_i F_\tau\right)_{,z}\left(L_j F_s\right)_{,y} dV \\
\mathbf{K}_{zz}^{\tau sij} &= C_{11}\int_V \left(L_i F_\tau\right)_{,z}\left(L_j F_s\right)_{,z} dV + C_{44}\int_V \left(L_i F_\tau\right)_{,x}\left(L_j F_s\right)_{,x} dV + C_{55}\int_V \left(L_i F_\tau\right)_{,y}\left(L_j F_s\right)_{,y} dV
\end{aligned}
\tag{27}
$$

where the partial derivatives with respect to x, y or z will be applied to the 3D function resulting from the product of the thickness function F and the shape function L, depending on the model.

The 3×3 fundamental nucleus of the mass matrix $\mathbf{M}^{\tau sij}$ is defined by its non-zero components:

$$
\mathbf{M}_{xx}^{\tau sij} = \mathbf{M}_{yy}^{\tau sij} = \mathbf{M}_{zz}^{\tau sij} = \rho \int_V \left(L_i F_\tau\right)\left(L_j F_s\right) dV \tag{28}
$$

where ρ is the density of the plate.

References

[1] S.M.B. Afonso, E. Hinton, Free vibration analysis and shape optimization of variable thickness plates and shells—i. Finite element studies, Comput. Syst. Eng. 6 (1) (1995) 27–45.
[2] P. Linde, Virtual testing of stiffened composite panels at airbus, Int. J. Struct. Stab. Dyn. 10 (04) (2010) 589–600.
[3] F.X. Irisarri, C. Julien, D. Bettebghor, F. Lavelle, Y. Guerin, K. Mathis, A general optimization strategy for composite sandwich structures, Struct. Multidiscip. Optim. 63 (6) (2021) 3027–3044.
[4] K.R. Kashyzadeh, S.S. Rahimian Koloor, M. Omidi Bidgoli, M. Petrů, A. Amiri Asfarjani, An optimum fatigue design of polymer composite compressed natural gas tank using hybrid finite element-response surface methods, Polymers 13 (4) (2021).
[5] F.J. Ramírez-Gil, E.C. Nelli Silva, W. Montealegre-Rubio, Through-thickness perforated steel plates optimized for ballistic impact applications, Mater. Des. 212 (2021) 110257.
[6] V.H. Cortinez, P.A.A. Laura, Analysis of vibrating rectangular plates of discontinuously varying thickness by means of the kantorovich extended method, J. Sound Vib. 137 (3) (1990) 457–461.
[7] P. Singhatanadgid, P. Taranajetsada, Vibration analysis of stepped rectangular plates using the extended kantorovich method, Mech. Adv. Mater. Struct. 23 (2) (2016) 201–215.
[8] H.C. Sanzi, A. Bergmann, R. Carnicer, P.A.A. Laura, Numerical experiments on vibrating rectangular plates with discontinuously varying cross sections, J. Sound Vib. 135 (1) (1989) 161–165.

[9] Ö. Civalek, Fundamental frequency of isotropic and orthotropic rectangular plates with linearly varying thickness by discrete singular convolution method, Appl. Math. Model. 33 (10) (2009) 3825–3835.
[10] S.K. Malhotra, N. Ganesan, M.A. Veluswami, Vibrations of orthotropic square plates having variable thickness (linear variation), Composites 19 (6) (1988) 467–472.
[11] A. Fallah, M.H. Kargarnovin, M.M. Aghdam, Free vibration analysis of symmetrically laminated fully clamped skew plates using extended kantorovich method, in: Composite Science and Technology, in: Key Engineering Materials, vol. 471, Trans Tech Publications Ltd, 2011, pp. 739–744, 6.
[12] F. Yekkalam Tash, B. Navayi Neya, An analytical solution for bending of transversely isotropic thick rectangular plates with variable thickness, Appl. Math. Model. 77 (2020) 1582–1602.
[13] B. Singh, V. Saxena, Axisymmetric vibration of a circular plate with double linear variable thickness, J. Sound Vib. 179 (5) (1995) 879–897.
[14] B. Singh, V. Saxena, Axisymmetric vibration of a circular plate with exponential thickness variation, J. Sound Vib. 192 (1) (1996) 35–42.
[15] T.Y. Wu, G.R. Liu, Free vibration analysis of circular plates with variable thickness by the generalized differential quadrature rule, Int. J. Solids Struct. 38 (44) (2001) 7967–7980.
[16] S. Azimi, Free vibration of circular plates with elastic edge supports using the receptance method, J. Sound Vib. 120 (1) (1988) 19–35.
[17] S. Azimi, Free vibration of circular plates with elastic or rigid interior support, J. Sound Vib. 120 (1) (1988) 37–52.
[18] C.M. Wang, G.M. Hong, T.J. Tan, Elastic buckling of tapered circular plates, Comput. Struct. 55 (6) (1995) 1055–1061.
[19] E. Bahmyari, A. Rahbar-Ranji, Free vibration analysis of orthotropic plates with variable thickness resting on non-uniform elastic foundation by element free galerkin method, J. Mech. Sci. Technol. 26 (9) (2012) 2685–2694.
[20] G.P. Vasiliev, A.L. Smirnov, Free vibration frequencies of a circular thin plate with variable parameters, Vestnik St. Petersburg Univ., Math. 53 (3) (2020) 351–357.
[21] E. Carrera, M. Cinefra, M. Petrolo, E. Zappino, Finite Element Analysis of Structures Through Unified Formulation, Wiley, 2014.
[22] G. Li, E. Carrera, M. Cinefra, A.G. de Miguel, A. Pagani, E. Zappino, An adaptable refinement approach for shell finite element models based on node-dependent kinematics, Composites B 210 (2019) 1–19.
[23] F. Moleiro, E. Carrera, E. Zappino, G. Li, M. Cinefra, Layerwise mixed elements with node-dependent kinematics for global–local stress analysis of multilayered plates using high-order legendre expansions, Comput. Methods Appl. Mech. Engrg. 359 (2020) 112764.
[24] G. Kirchhoff, Uber das gleichgewicht und die bewegung einer elastishen scheibe, Crelles J. 40 (1850) 51–88.
[25] E. Reissner, The effect of transverse shear deformation on the bending of elastic plates, J. Appl. Mech. 12 (1945) 69–76.
[26] R.D. Mindlin, Influence of rotatory inertia and shear in flexural motions of isotropic elastic plates, J. Appl. Mech. 18 (1951) 28–31.
[27] J.N. Reddy, A simple higher-order theory for laminated composite plates, J. Appl. Mech. 51 (4) (1984) 745–752.
[28] M. Cinefra, M.C. Moruzzi, Dynamic analysis of variable thickness shells in aerospace applications via cuf adaptive finite elements, in: ASME's 1st Annual Aerospace Structures, Structural Dynamics, and Materials Conference (SSDM) Proceedings, 2023.
[29] MC. Moruzzi, M. Cinefra, S. Bagassi, E. Zappino, Vibro-acoustic analysis of multi-layer cylindrical shell-cavity systems via cuf finite elements, in: 33th ICAS 2022 Proceedings, 2022.
[30] M. Cinefra, Non-conventional 1d and 2d finite elements based on cuf for the analysis of non-orthogonal geometries, Eur. J. Mech. A Solids 88 (2021) 104273.
[31] M. Cinefra, A. Rubino, Adaptive mesh using non-conventional 1d and 2d finite elements based on cuf, Mech. Adv. Mater. Struct. 30 (5) (2023) 1095–1105.
[32] K. Washizu, Variational Methods in Elasticity and Plasticity, Elsevier, Science & Technology, 1974.
[33] G.M. Kulikov, A.A. Mamontov, S.V. Plotnikova, S.A. Mamontov, Exact geometry solid-shell element based on a sampling surfaces technique for 3d stress analysis of doubly-curved composite shells, Curved Layered Struct. 3 (1) (2016).
[34] G.M. Kulikov, S.V. Plotnikova, A method of solving three-dimensional problems of elasticity for laminated composite plates, Mech. Compos. Mater. 48 (1) (2012) 15–26.
[35] A.J.M. Ferreira, C.M.C. Roque, E. Carrera, M. Cinefra, Analysis of thick isotropic and cross-ply laminated plates by radial basis functions and a unified formulation, J. Sound Vib. 330 (4) (2011) 771–787.
[36] E. Carrera, M. Cinefra, G. Li, G.M. Kulikov, Mitc9 shell finite elements with miscellaneous through-the-thickness functions for the analysis of laminated structures, Compos. Struct. 154 (2016) 360–373.
[37] E. Carrera, M. Cinefra, G. Li, Refined finite element solutions for anisotropic laminated plates, Compos. Struct. 183 (2018) 63–76, In honor of Prof. Y. Narita.
[38] M. Cinefra, M.C. Moruzzi, S. Bagassi, E. Zappino, E. Carrera, Vibro-acoustic analysis of composite plate-cavity systems via cuf finite elements, Compos. Struct. 259 (2021) 113428.
[39] R.B. Bhat, P.A.A. Laura, R.G. Gutierrez, V.H. Cortinez, H.C. Sanzi, Numerical experiments on the determination of natural frequencies of transverse vibrations of rectangular plates of non-uniform thickness, J. Sound Vib. 138 (2) (1990) 205–219.
[40] G.Z. Harris, The normal modes of a circular plate of variable thickness†, Quart. J. Mech. Appl. Math. 21 (3) (1968) 321–327, 08.
[41] J.W.S. Rayleigh, The Theory of Sound, I-II, second ed., Dover Publications, 1896.
[42] G. Petrone, V. D'Alessandro, F. Franco, S. De Rosa, Numerical and experimental investigations on the acoustic power radiated by aluminium foam sandwich panels, Compos. Struct. 118 (2014) 170–177.